ELSEVIER

Journal of Organometallic Chemistry 528 (1997) 19–33

Journal of Organometallic Chemistry

Electronic structure of f^1 lanthanide and actinide complexes. Part 2. [1] Non-relativistic and relativistic calculations of the ground state electronic structures and optical transition energies of $[Ce(\eta\text{-}C_5H_5)_3]$, $[Th(\eta\text{-}C_5H_5)_3]$ and $[Pa(\eta\text{-}C_8H_8)_2]$ [2]

Nikolas Kaltsoyannis [a,*], Bruce E. Bursten [b]

[a] *Department of Chemistry, University College London, 20 Gordon Street, London WC1H 0AJ, UK*
[b] *Department of Chemistry, The Ohio State University, Columbus, OH 43210, USA*

Received 13 March 1996; accepted 20 April 1996

Abstract

Non-relativistic and relativistic discrete variational-Xα calculations have been performed on $[Ce(\eta\text{-}C_5H_5)_3]$, $[Th(\eta\text{-}C_5H_5)_3]$ and $[Pa(\eta\text{-}C_8H_8)_2]$. Metal–ligand covalent interactions in $[Ce(\eta\text{-}C_5H_5)_3]$ and $[Th(\eta\text{-}C_5H_5)_3]$ are dominated by metal d-orbital participation in the $(\eta\text{-}C_5H_5)$ π_2-based 2e and 3e molecular orbitals, and an f-orbital contribution to the $1a_2$ level. The non-relativistic calculations predict formal ground configurations of $4f^1$ and $5f^1$ for $[Ce(\eta\text{-}C_5H_5)_3]$ and $[Th(\eta\text{-}C_5H_5)_3]$ respectively, while the destabilisation of the nf and slight stabilisation of the $(n+1)d\sigma$ level on the incorporation of relativistic effects result in a $6d^1$ electronic configuration for $[Th(\eta\text{-}C_5H_5)_3]$. $[Pa(\eta\text{-}C_8H_8)_2]$ is found to have a $5f^1$ ground configuration in both non-relativistic and relativistic calculations, and both the 6d and 5f metal orbitals participate significantly in metal–ligand covalent bonding. The 4f-based molecular orbitals of $[Ce(\eta\text{-}C_5H_5)_3]$ are found to be little altered from those of free Ce(III), and show a three-below-four ($j=5/2$ below $j=7/2$) spin–orbit coupling pattern. The greater radial extension of the 5f atomic orbitals and their closer energy match with vacant carbocyclic ring levels destroys this splitting pattern in $[Th(\eta\text{-}C_5H_5)_3]$ and $[Pa(\eta\text{-}C_8H_8)_2]$. The electronic absorption spectra of all three molecules have been calculated using the transition state method. In $[Ce(\eta\text{-}C_5H_5)_3]$ and $[Pa(\eta\text{-}C_8H_8)_2]$, the transitions are principally $f \rightarrow f$ in nature, although a low-lying $f \rightarrow d\sigma$ shift is predicted in both cases. In $[Ce(\eta\text{-}C_5H_5)_3]$, the calculated $f \rightarrow d\sigma$ transition is in good agreement with that found experimentally for $[Ce(\eta\text{-}C_5H_3(SiMe_3)_2)_3]$. The calculated spectrum of $[Th(\eta\text{-}C_5H_5)_3]$ consists of a series of $d \rightarrow f$ transitions, in agreement with the intense peaks observed in the experimental spectrum of $[Th(\eta\text{-}C_5H_3(SiMe_3)_2)_3]$. Comparison of the calculated transitions of $[Pa(\eta\text{-}C_8H_8)_2]$ with the experimental spectrum of $[Pa(\eta\text{-}C_8H_4(CH_3)_4)_2]$ suggests that the latter is due to charge transfer transitions and that the $f \rightarrow d\sigma$ shift has not yet been experimentally observed.

Keywords: f-Element; Electronic structure; Computation; Density functional; Relativistic

1. Introduction

We recently set out our aim of calculating electronic transition energies in complexes containing actinide elements [1], using a fully relativistic implementation of the discrete variational (DV)-Xα molecular orbital (MO) calculational method [2–4]. We described results obtained on the isovalent octahedral hexahalide complexes PaX_6^{2-} (X = F, Cl, Br, I), UX_6^- (X = F, Cl, Br) and NpF_6, which contain a single 5f electron. This initial study was highly encouraging, with quantitative agreement between theory and experiment being achieved in almost all cases.

In this paper, we turn our attention to rather different systems, and focus on three organometallic compounds; $[Ce(\eta\text{-}C_5H_5)_3]$, $[Th(\eta\text{-}C_5H_5)_3]$ and $[Pa(\eta\text{-}C_8H_8)_2]$. All

* Corresponding author.

[1] Part 1: N. Kaltsoyannis and B.E. Bursten, *Inorg. Chem.*, *34* (1995) 2735.

[2] Dedicated to Professor Malcolm L.H. Green – "le fromage le plus grand" – on the occasion of his 60th birthday.

PII S0022-328X(96)06406-6

of these molecules possess one metal-localised electron (i.e. contain the metal in a formal oxidation state one less than its "group valence"), and are therefore logical targets for extending our project. The increased complexity of the organometallic species over the octahedral hexahalide complexes presents an even greater challenge to the computational method, but we feel such a study to be justified in the light of our initial results.

The absorption spectra of the title compounds are expected to be particularly interesting given the energetic proximity of the metal valence atomic orbitals (AOs) at the start of the lanthanide and actinide series. This energetic closeness should give rise to spectra that do not consist solely of f → f transitions, but which may contain low energy f → d shifts. Indeed the ground electronic configuration of $[Th(\eta\text{-}C_5H_3(SiMe_3)_2)_3]$ has been shown to be $6d^1$ rather than $5f^1$ [5], which has major consequences for its optical spectroscopy [6]. The spectrum of $[Ce(\eta\text{-}C_5H_3(SiMe_3)_2)_3]$ has also been measured [6], thereby providing an experimental comparison with our results on the closely related unsubstituted cyclopentadienyl analogues. A similar situation exists for protactinocene; the spectrum of the unsubstituted compound has not been measured but that of $[Pa(\eta\text{-}C_8H_4(CH_3)_4)_2]$ has [7], again allowing us to compare experimental and theoretical data.

A second, though no less important, aim of this work is to compare the results of the DV-Xα method with our previously reported quasi-relativistic scattered wave (SW)-Xα investigations of $[M(\eta\text{-}C_5H_5)_3]$ (M = Ln, An) [8–11]. It is generally agreed that the 4f AOs are more shielded from the ligand environment than their 5f counterparts [12–14], with the consequence that metal–ligand f-orbital covalency is more extensive in organoactinides than organolanthanides. The situation is less clear cut when it comes to the 5d and 6d AOs, and recent work [11,12] has suggested that the overall covalent interaction in organolanthanide compounds is greater than initially concluded [15]. Much work has also been performed on the electronic structure of actinocenes [16–27], with the extent of 6d- versus 5f-orbital covalency being one of the principal issues addressed. Our work is naturally compared with previous studies, although we focus on the aspects of the electronic structure most relevant to the optical spectroscopy of $[Pa(\eta\text{-}C_8H_8)_2]$.

The paper is divided into two main sections. In Section 3.1 we develop a bonding model for $[M(\eta\text{-}C_5H_5)_3]$ compounds, and discuss the predicted electronic absorption spectra of $[Ce(\eta\text{-}C_5H_5)_3]$ and $[Th(\eta\text{-}C_5H_5)_3]$ within that model. Comparison with the experimental data available on $[Ce(\eta\text{-}C_5H_3(SiMe_3)_2)_3]$ and $[Th(\eta\text{-}C_5H_3(SiMe_3)_2)_3]$ is also made. In Section 3.2 we focus on $[Pa(\eta\text{-}C_8H_8)_2]$, and discuss its absorption spectrum in relation to the experimental data available for $[Pa(\eta\text{-}C_8H_4(CH_3)_4)_2]$.

2. Computational details

The computational methodology used in our investigations was set out in the companion paper to this study [1], and we will not repeat it here. The metal–$(\eta\text{-}C_5H_5)$ centroid distances were as used in our previous work [11], i.e. 2.80 Å for $[Th(\eta\text{-}C_5H_5)_3]$ and 2.79 Å for $[Ce(\eta\text{-}C_5H_5)_3]$. The metal–ring distance employed for $[Pa(\eta\text{-}C_8H_8)_2]$ was 1.958 Å, this being half way between the experimental values for $[Th(\eta\text{-}C_8H_8)_2]$ and $[U(\eta\text{-}C_8H_8)_2]$ [28]. All calculations were performed on the Cray Y-MP/864 supercomputer at the Ohio Supercomputing Centre. The results are presented pictorially via energy-level diagrams. Tabulated MO eigenvalues and percentage AO compositions are available as supplementary material.

3. Results and discussion

3.1. $[Ce(\eta\text{-}C_5H_5)_3]$ and $[Th(\eta\text{-}C_5H_5)_3]$

Both $[Ce(\eta\text{-}C_5H_3(SiMe_3)_2)_3]$ [29] and $[Th(\eta\text{-}C_5H_3(SiMe_3)_2)_3]$ [30] have been shown to possess structures in which the metal atom and the centroids of the substituted cyclopentadienyl rings are coplanar, and the solution electronic absorption spectra of both compounds have been measured [6]. Calculations on $[Ce(\eta\text{-}C_5H_3(SiMe_3)_2)_3]$ and $[Th(\eta\text{-}C_5H_3(SiMe_3)_2)_3]$ would be prohibitively demanding, and we have chosen instead to investigate the unsubstituted $[Ce(\eta\text{-}C_5H_5)_3]$ and $[Th(\eta\text{-}C_5H_5)_3]$. Not only does this simplification facilitate comparison with our previous SW-Xα calculations on $[M(\eta\text{-}C_5H_5)_3]$ (M = Ln, An) [8–11], but it is unlikely that replacement of the $(\eta\text{-}C_5H_3(SiMe_3)_2)$ rings with $(\eta\text{-}C_5H_5)$ units would significantly modify any essentially metal-localised electronic transitions. We therefore expect that a comparison of our calculated spectra of $[Ce(\eta\text{-}C_5H_5)_3]$ and $[Th(\eta\text{-}C_5H_5)_3]$ with the experimentally determined values for $[Ce(\eta\text{-}C_5H_3(SiMe_3)_2)_3]$ and $[Th(\eta\text{-}C_5H_3(SiMe_3)_2)_3]$ will be a productive exercise. Before discussing the spectra, we present a summary of the bonding in $[M(\eta\text{-}C_5H_5)_3]$ systems and a comparison of the SW- and DV-Xα results.

3.1.1. Bonding in $[Ce(\eta\text{-}C_5H_5)_3]$ and $[Th(\eta\text{-}C_5H_5)_3]$

In previous accounts, we have approached the bonding in $[M(\eta\text{-}C_5H_5)_3]$ (M = Ln, An) complexes using both the C_{3v} [9] and D_{3h} [11] point groups. Although the highest possible symmetry of an $[M(\eta\text{-}C_5H_5)_3]$ system in which the metal atom and the $(\eta\text{-}C_5H_5)$ ring centroids are coplanar is C_{3v}, the metal–$(\eta\text{-}C_5H_5)$ bonding has been found to exhibit only minor deviations from virtual D_{3h} symmetry. The higher symmetry of the latter point group has been employed in order to clarify discussion of the metal–ring bonding [11]. In the

work reported here, we adopt the C_{3v} point group as the basis for our discussion, although we relate the C_{3v} orbitals to their D_{3h} counterparts to aid comparison with our earlier work.

The interactions of an $(\eta\text{-}C_5H_5)_3$ ligand field and a central metal have been discussed in some detail previously [9,11,31]. The principal metal–ring bonding occurs between the valence AOs of the central atom and the highest occupied e_1'' (π_2) orbitals of the D_{5h} (η-C_5H_5) ligands. A lesser interaction takes place between the metal orbitals and the most stable a_2'' (π_1) level of the (η-C_5H_5) rings. In a C_{3v} $(\eta\text{-}C_5H_5)_3$ ligand field, the (η-C_5H_5) π_1 orbitals give rise to $a_1 + e$ symmetry combinations ($a_1' + e'$ in D_{3h}), while the π_2 levels result in $a_1 + a_2 + 2e$ ($a_2' + e' + a_2'' + e''$ in D_{3h}) orbitals. These π_2-derived levels are strongly split by ligand–ligand interactions, with the a_2 (a_2') [32] orbital being significantly destabilised above the other combinations. This description immediately provides an elegant rationalisation of the paucity of the $[M(\eta\text{-}C_5H_5)_3]$

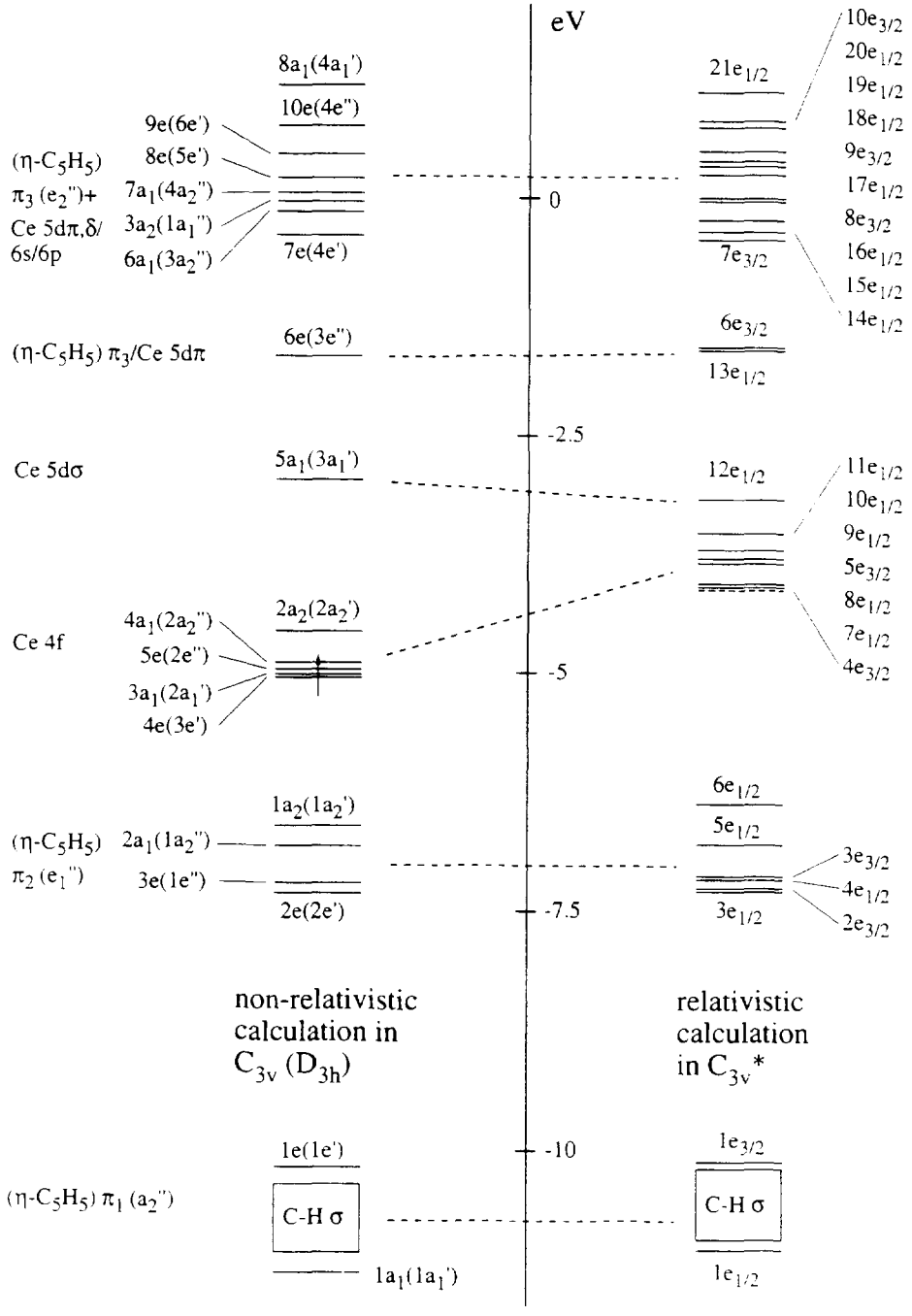

Fig. 1. Molecular orbital scheme for $[Ce(\eta\text{-}C_5H_5)_3]$. The dashed lines are designed to indicate broadly how the non-relativistic MOs relate to their relativistic counterparts.

unit when M is a transition metal, and the abundance of the same unit in which the metal possesses valence f orbitals. There is no d orbital that transforms as a_2 symmetry in C_{3v} ligand environments; in contrast the $f_{y(3x^2-y^2)}$ orbital can stabilise the ligand a_2 combination and provide significant metal–ligand bonding in the process.

Non-relativistic calculations. Although it is widely recognised that it is necessary to incorporate relativistic considerations when calculating the electronic structure of heavy element complexes [33–35], we begin our analysis with the results from non-relativistic calculations on $[Ce(\eta\text{-}C_5H_5)_3]$ and $[Th(\eta\text{-}C_5H_5)_3]$. The principal features of the metal–ligand interactions are present in such an approach, and we feel it is helpful to retain the chemically familiar single point group notation for as long as possible. The results of these calculations are presented in Fig. 1 ($[Ce(\eta\text{-}C_5H_5)_3]$) and 2 ($[Th(\eta\text{-}C_5H_5)_3]$).

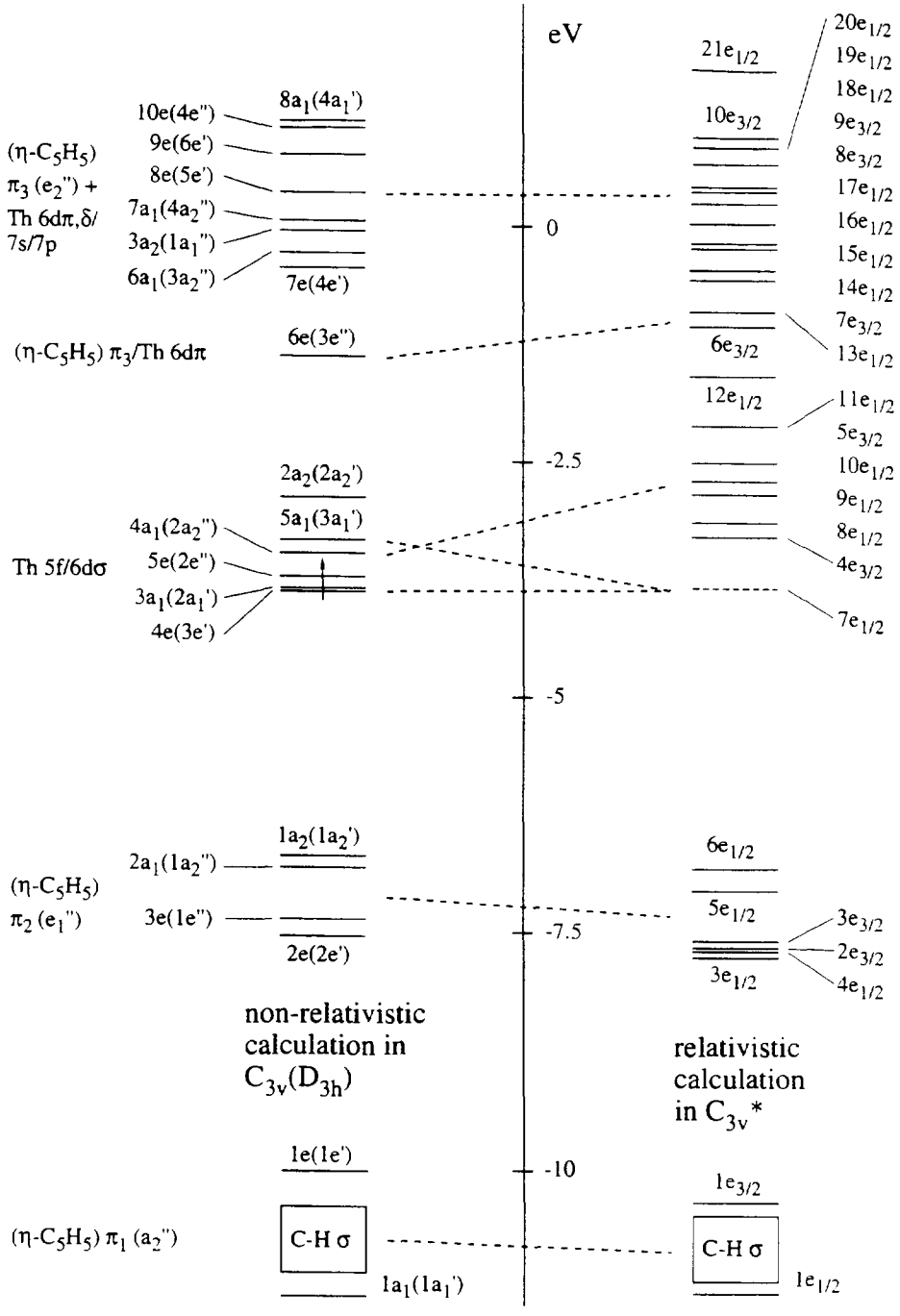

Fig. 2. Molecular orbital scheme for $[Th(\eta\text{-}C_5H_5)_3]$. The dashed lines are designed to indicate broadly how the non-relativistic MOs relate to their relativistic counterparts.

Turning first to $[Ce(\eta\text{-}C_5H_5)_3]$, at most negative eigenvalues come the $(\eta\text{-}C_5H_5)$ π_1-derived orbitals, the $1a_1$ ($1a'_1$) and 1e (1e'), which sandwich a group of C–H ring σ bonding levels. There is then a gap to the π_2-based MOs, and subsequently to the Ce 4f manifold, which contains one electron. In keeping with our earlier assertion of a significant a_2 symmetry metal–ligand interaction, the $2a_2$ ($2a'_2$) orbital is destabilised above the other 4f-based levels and has greater C character.

The principal component of the vacant $5a_1$ ($3a'_1$) MO is the Ce $5d\sigma$ orbital. $5d\pi$ and $5d\delta$ character is distributed among the (6e (3e'') and 10e (4e'')) and (7e (4e') and 9e (6e')) levels respectively, all of which lie well removed from the $5a_1$ ($3a'_1$) MO in energy. As the d_{z^2} orbital lies along the principal axis of the molecule, it experiences far less interaction with the $(\eta\text{-}C_5H_5)$ rings than the remaining d orbitals. Consequently it is much less destabilised, an effect that has a major impact on both the ground and excited state electronic structure and the electronic absorption spectra of $[Ce(\eta\text{-}C_5H_5)_3]$ and $[Th(\eta\text{-}C_5H_5)_3]$.

The 6e (3e'') through $8a_1$ ($4a'_1$) orbitals are mixtures of the remaining metal valence levels and the ligand combinations derived from the e''_2 (π_3) orbitals of the $(\eta\text{-}C_5H_5)$ rings. They lie some considerable distance away from the Ce 4f manifold in energy terms, and are not expected to be a factor in the electronic absorption spectrum of $[Ce(\eta\text{-}C_5H_5)_3]$.

The non-relativistic calculation on $[Th(\eta\text{-}C_5H_5)_3]$ (Fig. 2) is in many ways similar to its lanthanide analogue. The $(\eta\text{-}C_5H_5)$ π_1- and π_2-based levels show the same orbital ordering, and have similar eigenvalues. The major difference between the two calculations comes in the metal-localised MOs. The Th 5f AOs are less stable than the Ce 4f AOs [36], with the result that there is a mixing of the Th 5f and $6d\sigma$ orbitals. Both the $3a_1$ ($2a'_1$) and $5a_1$ ($3a'_1$) MOs of $[Th(\eta\text{-}C_5H_5)_3]$ contain appreciable $6d_{z^2}$ character. Subsequently we find the 6e (3e'')–$8a_1$ ($4a'_1$) levels, which are once again similar to the $[Ce(\eta\text{-}C_5H_5)_3]$ equivalents – mixtures of $(\eta\text{-}C_5H_5)\pi_3$ with Th $6d\pi$, $6d\delta$, 7s and 7p.

Relativistic calculations. In order to proceed with a more detailed analysis and to permit meaningful comparison with the previous quasi-relativistic SW-Xα calculations, it is necessary to address the relativistic calculations. There are two major consequences of the incorporation of relativistic quantum mechanics into the calculation of the electronic structure of heavy element complexes. The first is the significant modification of the valence AO energies as a result of the stabilisation of the inner core s and p electrons, which are moving at classical velocities that are appreciable fractions of the speed of light. The effect on the valence orbitals is to slightly contract the s and p levels and to destabilise the more diffuse d and f functions, which experience reduced nuclear charge due to increased shielding by the s and p electrons [34]. The second consequence is the coupling of the electron's intrinsic spin angular momentum with that imposed by its orbital motion, an effect that is increasingly important for heavy element systems. All electronic states in such complexes are therefore properly characterised by non-integral angular momentum values, and must be described using double point group symmetry notation [37]. For the C_{3v} point group, the most significant effect of spin–orbit coupling is the lifting of the degeneracy of the e orbitals. The relationship between the spatial MOs of the C_{3v} point group and the spin-orbitals of the C^*_{3v} double group are given in Table 1.

The relativistic calculation results are shown on the right-hand sides of Figs. 1 and 2. The dashed lines linking the left- and right-hand sides of the figures are intended to indicate broadly how the non-relativistic MOs relate to their relativistic counterparts [38].

The effects of relativity on $[Ce(\eta\text{-}C_5H_5)_3]$ are significant only in the metal-localised orbitals; the $(\eta\text{-}C_5H_5)$ π_1- and π_2-derived levels are perturbed only slightly. The Ce 4f manifold, however, is significantly destabilised, bringing it into closer energetic proximity with the $12e_{1/2}$ (predominantly Ce $5d\sigma$) orbital. This is expected to have a significant effect on the absorption spectrum of $[Ce(\eta\text{-}C_5H_5)_3]$, which is discussed below.

The observation of only minor perturbations to the ligand-localised levels on moving from C_{3v} to C^*_{3v} is also true of $[Th(\eta\text{-}C_5H_5)_3]$ (Fig. 2). The closer non-relativistic proximity of metal 5f and $6d\sigma$ orbitals, however, results in major changes to the metal-localised MOs in the relativistic calculation. Indeed, the calculation indicates that the predominantly $6d\sigma$ MO ($7e_{1/2}$) is the highest occupied molecular orbital (HOMO) of $[Th(\eta\text{-}C_5H_5)_3]$, with the 5f manifold ($4e_{3/2}$–$12e_{1/2}$) being destabilised above it. This change is highly significant for the electronic absorption spectrum: the non-relativistic calculation predicts that it should consist of a series of $f \rightarrow f/d$ transitions, whereas the relativistic calculation indicates a $d \rightarrow f$ spectrum. We will address this issue later; at this point we note only that our prediction of a $6d^1$ ground state for $[Th(\eta\text{-}C_5H_5)_3]$ is in complete agreement with previous work, both theoretical [8] and experimental [5,6], and that $[Ce(\eta\text{-}C_5H_5)_3]$ and $[Th(\eta\text{-}C_5H_5)_3]$ are predicted to have significantly different ground states, $4f^1$ and $6d^1$ respectively.

Table 1
Relationship between the irreducible representations of the C_{3v} single and C^*_{3v} double point groups

C_{3v}	C^*_{3v}
a_1	$e_{1/2}$
a_2	$e_{1/2}$
e	$e_{1/2}+e_{3/2}$

We now turn to a more detailed examination of the valence MOs of $[Ce(\eta\text{-}C_5H_5)_3]$ and $[Th(\eta\text{-}C_5H_5)_3]$, beginning with the $(\eta\text{-}C_5H_5)$ π_2-based orbitals, which provide the principal source of metal–$(\eta\text{-}C_5H_5)$ bonding. In our previous SW-Xα calculations on $[Ln(\eta\text{-}C_5H_5)_3]$ and $[An(\eta\text{-}C_5H_5)_3]$, we concluded that for the early lanthanide and actinide metals, the major metal contributions to the 2e (2e′) and 3e (1e″) levels were the dδ and dπ orbitals respectively, with only a very small f orbital participation. 15% 5dδ AO character was found for the 2e MO of $[Pr(\eta\text{-}C_5H_5)_3]$, versus only 1% 4f, with similar values for the early actinides. The 5dπ/4fδ ratio for the 3e MO of $[Ce(\eta\text{-}C_5H_5)_3]$ was found to be 85:15, with a total metal participation of ca. 25%. Although the reduction in the number of irreducible representations to two in C_{3v}^* makes separation of the type of interaction into π/δ less valid, we may still compare relative d and f orbital contributions to the relativistic counterparts of the 2e (2e′) and 3e (1e″) orbitals. In $[Ce(\eta\text{-}C_5H_5)_3]$, the $3e_{1/2}$ and $2e_{3/2}$ MOs have 10.47% 5d, 0.28% 4f and 10.71% 5d, 0.22% 4f contributions respectively, while the $4e_{1/2}$ and $3e_{3/2}$ orbitals reveal slightly greater metal character with a small increase in the relative contribution of the 4f orbitals (13.47% 5d, 1.55% 4f and 13.15% 5d, 1.77% 4f). In $[Th(\eta\text{-}C_5H_5)_3]$, all four of these levels show marginally increased amounts of metal character relative to the Ce complex, ranging from 13.07% 6d, 0.68% 5f in the $3e_{3/2}$ level to 15.04% 6d, 1.41% 5f in the $4e_{1/2}$ MO. The DV- and SW-Xα calculations are therefore in agreement as to the type of interaction in the most stable $(\eta\text{-}C_5H_5)$ π_2-based orbitals, although the DV calculations predict slightly less metal participation.

The $1a_2$ ($1a_2'$) orbital of $[Ce(\eta\text{-}C_5H_5)_3]$ was calculated by the SW method to contain 28% Ce 4f character, and a similar contribution was found for the equivalent orbital of the early actinides. The relativistic counterparts of these orbitals are the $6e_{1/2}$ levels of both $[Ce(\eta\text{-}C_5H_5)_3]$ and $[Th(\eta\text{-}C_5H_5)_3]$ and, while there is little symmetry restriction, the only significant metal contributions come from the f orbitals. The percentages are much reduced from the SW calculations, at 10.90% 4f for $[Ce(\eta\text{-}C_5H_5)_3]$ and 9.77% 5f in $[Th(\eta\text{-}C_5H_5)_3]$.

The remaining $(\eta\text{-}C_5H_5)$ π_2-based orbital is the $5e_{1/2}$ level, the relativistic counterpart of the $2a_1$ ($1a_2''$) MO. This orbital is found to contain only small metal contributions in both complexes, 3.28% 4f, 2.91% 6p in $[Ce(\eta\text{-}C_5H_5)_3]$ and 3.13% 5f, 2.22% 7p in $[Th(\eta\text{-}C_5H_5)_3]$.

The degree of metal involvement in the $(\eta\text{-}C_5H_5)$ π_2-based orbitals may be taken as an estimate of the degree of metal–ligand covalency. Nugent et al. [15] concluded that the bonding in $[Ln(\eta\text{-}C_5H_5)_3]$ (Ln = Pr, Nd, Er) consisted of ca. 3% or less covalent character, based on a study of solid-state UV–visible spectra. A slightly greater covalency was estimated for $[Am(\eta\text{-}C_5H_5)_3]$ and $[Cm(\eta\text{-}C_5H_5)_3]$. Subsequently Hazin et al. [12] used luminescence spectroscopy on a range of Ce compounds to suggest that the bonding in $[Ce(\eta\text{-}C_5H_5)_3]$ is approximately 10% covalent and is due largely to the 5d orbitals. This conclusion is in excellent agreement with the results of our calculations on $[Ce(\eta\text{-}C_5H_5)_3]$, which find an average of 11.92% metal participation in the $3e_{1/2}$–$6e_{1/2}$ $(\eta\text{-}C_5H_5)$ π_2-based MOs. The equivalent levels of $[Th(\eta\text{-}C_5H_5)_3]$ reveal a slightly greater average metal contribution, 13.21%, as mentioned above.

The $4e_{3/2}$–$11e_{1/2}$ MOs of $[Ce(\eta\text{-}C_5H_5)_3]$ form the metal-localised 4f manifold. It is noticeable that there is a three-below-four splitting of these orbitals, perturbed only slightly by the destabilisation of the metal–$(\eta\text{-}C_5H_5)$ antibonding $11e_{1/2}$ level above the rest (the relativistic equivalent of the $2a_2$ ($2a_2'$) orbital). The three-below-four splitting is as expected from spin–orbit coupling of a free atom $4f^1$ configuration; a six-fold degenerate $j = 5/2$ block below an eight-fold degenerate $j = 7/2$ group [39]. Indeed, if we analyse the 4f manifold of $[Ce(\eta\text{-}C_5H_5)_3]$ we find the $4e_{3/2}$–$8e_{1/2}$ MOs to have predominant f ($j = 5/2$) characteristics with the $9e_{1/2}$–$11e_{1/2}$ being mainly f ($j = 7/2$) in composition. This analysis provides evidence that the Ce 4f orbitals are little perturbed by interaction with the $(\eta\text{-}C_5H_5)_3$ ligand field, and split in a manner analogous to that expected of a free Ce atom, a widespread observation in lanthanide-containing compounds [13,14]. The composition of the $4e_{3/2}$–$10e_{1/2}$ MOs further supports this notion, all of them being > 90% Ce 4f in character [40]. The one exception is the $11e_{1/2}$ MO, which contains a reduced metal contribution on account of the interaction between the $f_{y(3x^2-y^2)}$ (in non-relativistic notation) orbital and the $(\eta\text{-}C_5H_5)$ π_2 a_2 level.

The $12e_{1/2}$ MO of $[Ce(\eta\text{-}C_5H_5)_3]$, the relativistic equivalent of the $5a_1$ ($3a_1'$) level, is found to be 63.81% Ce 5d and 14.10% 6s in character, a 82:18 d:s ratio in the metal contribution. This represents a significant change from the non-relativistic calculation, in which a 93:7 d:s ratio is observed. The stabilisation of the Ce 6s AO with respect to the 5d on the incorporation of relativity results in greater d/s mixing and a slight stabilisation of the $12e_{1/2}$ MO over the $5a_1$ ($3a_1'$).

It is difficult to make similar comparison of the d/s ratio of the equivalent non-relativistic a_1 orbital of $[Th(\eta\text{-}C_5H_5)_3]$, as both the $3a_1$ ($2a_1'$) and $5a_1$ ($3a_1'$) MOs contain appreciable d and f character and only the $5a_1$ ($3a_1'$) has any s character (5.68%). The $7e_{1/2}$ HOMO of relativistic $[Th(\eta\text{-}C_5H_5)_3]$, however, contains 66.16% 6d and only 5.13% 7s, a d:s ratio (93:7) which is somewhat greater than in the $12e_{1/2}$ of $[Ce(\eta\text{-}C_5H_5)_3]$.

The splitting of the Th 5f manifold in $[Th(\eta\text{-}C_5H_5)_3]$ is less clear cut than the Ce case, with no discernable three-below-four pattern. Furthermore, the separation of

Table 2
Calculated relativistic electronic transition energies in $[Ce(\eta\text{-}C_5H_5)_3]$; experimental values for $[Ce(\eta\text{-}C_5H_3(SiMe_3)_2)_3]$ from Ref. [6]

Transition	Transition type [a]	Energy
(i) $[Ce(\eta\text{-}C_5H_5)_3]$, calculated		
$(4e_{3/2} + 7e_{1/2} + 8e_{1/2}) \rightarrow 5e_{3/2}$	$Ce4\bar{f} \rightarrow Ce4f$	2450 cm^{-1} (0.304 eV)
$(4e_{3/2} + 7e_{1/2} + 8e_{1/2}) \rightarrow 9e_{1/2}$	$Ce4\bar{f} \rightarrow Ce4f$	2791 cm^{-1} (0.364 eV)
$(4e_{3/2} + 7e_{1/2} + 8e_{1/2}) \rightarrow 10e_{1/2}$	$Ce4\bar{f} \rightarrow Ce4f$	3777 cm^{-1} (0.468 eV)
$(4e_{3/2} + 7e_{1/2} + 8e_{1/2}) \rightarrow 11e_{1/2}$	$Ce4\bar{f} \rightarrow Ce4f/4\bar{f}$	7231 cm^{-1} (0.897 eV)
$(4e_{3/2} + 7e_{1/2} + 8e_{1/2}) \rightarrow 12e_{1/2}$	$Ce4\bar{f} \rightarrow Ce5d/5\bar{d}/6s$	16542 cm^{-1} (2.051 eV)
$6e_{1/2} \rightarrow (4e_{3/2} + 7e_{1/2} + 8e_{1/2})$	$(\eta\text{-}C_5H_5)\pi_2 \rightarrow Ce4\bar{f}$	26554 cm^{-1} (3.292 eV)
$(4e_{3/2} + 7e_{1/2} + 8e_{1/2}) \rightarrow 13e_{1/2}$	$Ce4\bar{f} \rightarrow (\eta\text{-}C_5H_5)\pi_3/Ce5\bar{d}/5d$	27660 cm^{-1} (3.429 eV)
(ii) $[Ce(\eta\text{-}C_5H_3(SiMe_3)_2)_3]$, experimental		
	$Ce4f \rightarrow Ce5d$	17650 cm^{-1}
	$Ce4f \rightarrow Ce5d$	22125 cm^{-1}
	metal → ligand charge transfer	> 25000 cm^{-1}

[a] Unbarred labels refer to the higher angular momentum j-based atomic orbital, barred to the lower.

atomic character into $\bar{f}$ below f is less complete, particularly in the $8e_{1/2}$ orbital, which is found to be a mixture of f, $\bar{f}$, $\bar{d}$ and d. The greater radial extension of the Th 5f orbitals versus the Ce 4f and their closer energetic proximity to the $(\eta\text{-}C_5H_5)$ π_3-based levels and the remaining metal valence orbitals results in the $[Th(\eta\text{-}C_5H_5)_3]$ 5f manifold being much less atom-like than the $[Ce(\eta\text{-}C_5H_5)_3]$ equivalent. The *minimum* C character of any of the $4e_{3/2}$–$11e_{1/2}$ MOs of $[Th(\eta\text{-}C_5H_5)_3]$ is 6.81% ($11e_{1/2}$), with substantially greater contributions in other cases, while the *maximum* C content of the equivalent orbitals of $[Ce(\eta\text{-}C_5H_5)_3]$ is 4.36% ($9e_{1/2}$). This greater metal/ligand mixing in $[Th(\eta\text{-}C_5H_5)_3]$ destroys the three-below-four splitting pattern, although some of the atomic grouping is retained in the complex, with the principal components of the $10e_{1/2}$–$12e_{1/2}$ MOs coming from the $j = 7/2$ manifold.

It should also be noted that the spread of f-based MO energies is greater in $[Th(\eta\text{-}C_5H_5)_3]$ than $[Ce(\eta\text{-}C_5H_5)_3]$. If we leave aside the $11e_{1/2}$ level of $[Ce(\eta\text{-}C_5H_5)_3]$ and the $12e_{1/2}$ MO of $[Th(\eta\text{-}C_5H_5)_3]$, which are the metal–ring antibonding counterparts of the $6e_{1/2}$ orbitals, the energy separation of the $4e_{3/2}$ and $10e_{1/2}$ in the lanthanide complex is 0.389 eV, but that between the $4e_{3/2}$ and $11e_{1/2}$ MOs of $[Th(\eta\text{-}C_5H_5)_3]$ is 1.089 eV. Both the increased spin–orbit coupling of the 5f versus the 4f AOs and the greater metal/ligand mixing in $[Th(\eta\text{-}C_5H_5)_3]$ contribute to this effect.

In summary, our DV-Xα calculations support many of the earlier assertions as to the bonding in $[M(\eta\text{-}$

Table 3
Calculated relativistic electronic transition energies in $[Th(\eta\text{-}C_5H_5)_3]$; experimental values for $[Th(\eta\text{-}C_5H_3(SiMe_3)_2)_3]$ from Ref. [6]

Transition	Transition type [a]	Energy
(i) $[Th(\eta\text{-}C_5H_5)_3]$, calculated		
$7e_{1/2} \rightarrow 4e_{3/2}$	$Th\ 6d/6\bar{d} \rightarrow Th\ 5\bar{f}/6d$	7004 cm^{-1} (0.868 eV)
$7e_{1/2} \rightarrow 8e_{1/2}$	$Th\ 6d/6\bar{d} \rightarrow Th\ 5f/5\bar{f}/6d$	7520 cm^{-1} (0.932 eV)
$7e_{1/2} \rightarrow 9e_{1/2}$	$Th\ 6d/6\bar{d} \rightarrow Th\ 5\bar{f}/5f$	13658 cm^{-1} (1.693 eV)
$7e_{1/2} \rightarrow 10e_{1/2}$	$Th\ 6d/6\bar{d} \rightarrow Th\ 5f$	14497 cm^{-1} (1.797 eV)
$7e_{1/2} \rightarrow 5e_{3/2}$	$Th\ 6d/6\bar{d} \rightarrow Th\ 5f/5\bar{f}$	15576 cm^{-1} (1.931 eV)
$7e_{1/2} \rightarrow 11e_{1/2}$	$Th\ 6d/6\bar{d} \rightarrow Th\ 5f$	19121 cm^{-1} (2.371 eV)
$7e_{1/2} \rightarrow 12e_{1/2}$	$Th\ 6d/6\bar{d} \rightarrow Th\ 5f/5\bar{f}$	27053 cm^{-1} (3.354 eV)
$7e_{1/2} \rightarrow 6e_{3/2}$	$Th\ 6d/6\bar{d} \rightarrow Th\ 5f/5\bar{f}/6d/(\eta\text{-}C_5H_5)\pi_3$	25461 cm^{-1} (3.157 eV)
$6e_{1/2} \rightarrow 7e_{1/2}$	$(\eta\text{-}C_5H_5)\pi_2 \rightarrow Th\ 6d/6\bar{d}$	26536 cm^{-1} (3.290 eV)
(ii) $[Th(\eta\text{-}C_5H_3(SiMe_3)_2)_3]$, experimental		
	Th 6d → Th 5f	15250 cm^{-1}
	Th 6d → Th 5f	16950 cm^{-1}
	Th 6d → Th 5f	19800 cm^{-1}
	Th 6d → Th 7s (?)	27800 cm^{-1}
	metal → ligand charge transfer	> 29000 cm^{-1}

[a] Unbarred labels refer to the higher angular momentum j-based atomic orbital, barred to the lower.

$C_5H_5)_3$] complexes. However, while it is valuable to be able to compare SW and DV calculations in some depth, the major aim of our current project is the calculation of electronic excitation energies, and it is to this that we now turn.

3.1.2. Electronic excitation energies in [Ce(η-$C_5H_5)_3$] and [Th(η-$C_5H_5)_3$]

Tables 2 and 3 present the calculated electronic excitation energies for [Ce(η-$C_5H_5)_3$] and [Th(η-$C_5H_5)_3$]. In both systems a separate transition state calculation [41] has been performed for each electronic transition. Also given are the experimental data for the closely related [Ce(η-$C_5H_3(SiMe_3)_2)_3$] and [Th(η-$C_5H_3(SiMe_3)_2)_3$] [6].

Although the calculated $7e_{1/2}$ HOMO of [Th(η-$C_5H_5)_3$] lies 0.535 eV from the $4e_{3/2}$ lowest unoccupied molecular orbital (LUMO), there is only 0.012 eV between the $4e_{3/2}$ and $7e_{1/2}$ MOs of [Ce(η-$C_5H_5)_3$], and the $8e_{1/2}$ orbital is a mere 0.034 eV further away. These levels form the Ce 4f̄ manifold, and the energies between them are so small that there would undoubtedly be a significant population of all three at room temperature. Indeed, in order to converge the [Ce(η-$C_5H_5)_3$] calculations it proved necessary to employ a thermal spreading factor [3], which puts a Fermi distribution of occupations on the MOs, thereby mimicking the "smearing" of the single f-based electron within the f̄ manifold. In calculating transition energies, a total of half an electron was removed from the $4e_{3/2}$, $7e_{1/2}$ and $8e_{1/2}$ MOs according to their population in the ground state calculation. Transition energies were then determined as the difference between the energy of the orbital to which promotion was made and the energies of the f̄ orbitals weighted according to their populations in the transition state calculation. Such an approach was not required for [Th(η-$C_5H_5)_3$], for which there is a larger HOMO–LUMO gap.

[Ce(η-$C_5H_5)_3$]. The calculated absorption spectrum of [Ce(η-$C_5H_5)_3$] has four transitions at low energy, corresponding to promotion of the f̄ ($j = 5/2$) electron to the MOs making up the f ($j = 7/2$) manifold. The first three of these lie in a narrow energy range (ca. 1300 cm^{-1}) with the transition to the $11e_{1/2}$ MO at somewhat greater energy, in accord with its ground state destabilisation via interaction with the (η-C_5H_5) π_2 orbitals. The next predicted shift is the f̄ → $12e_{1/2}$ (predominantly Ce 5d) transition, at 16542 cm^{-1}. It should be noted that in the ground state calculation the $12e_{1/2}$ orbital lies only 7856 cm^{-1} above the $4e_{3/2}$ level, illustrating how ground state eigenvalues are not always reliable guides to transition energies, especially when the MOs involved in the transition have different localisation properties.

There are no other predicted electronic transitions before the onset of charge transfer transitions. The ligand → metal, (η-C_5H_5) π_2 → Ce 4f̄ and metal → ligand, Ce 4f̄ → (η-C_5H_5) π_3 charge transfer transitions are calculated to occur within 1000 cm^{-1} of each other, between ca. 26500 and 27500 cm^{-1}. The predicted absorption spectrum of [Ce(η-$C_5H_5)_3$] thus consists of four weak f̄ → f transitions between ca. 2450 and 7250 cm^{-1}, a much more intense f̄ → d/d̄ shift at 16542 cm^{-1} and a charge transfer series beginning at ca. 26500 cm^{-1}. Although both $e_{1/2} \rightarrow e_{1/2}$ and $e_{1/2} \rightarrow e_{3/2}$ shifts are dipole-allowed in C_{3v}^*, many of the familiar factors governing the oscillator strengths of electronic transitions still apply, i.e. f ↔ f transitions are weak, f ↔ d much stronger and charge transfer transitions have very high absorption probabilities.

The absorption spectrum of [Ce(η-$C_5H_5)_3$] has not been measured, although that of the related [Ce(η-$C_5H_3(SiMe_3)_2)_3$] has [6]. It consists of two intense peaks in the 14000–25000 cm^{-1} range, centred at 17650 and 22125 cm^{-1} respectively. No data are provided below 14000 cm^{-1}, and 25000 cm^{-1} sees the onset of a very intense peak which is presumably a charge transfer transition of some type. It is not expected that substitution of two of the H atoms of the (η-C_5H_5) rings with $SiMe_3$ groups should have a pronounced effect upon the essentially metal-localised electronic promotions.

It is somewhat difficult to relate the experimental assignment to the calculated spectrum in that the former makes no mention of f → f shifts and considers the assignment only in terms of the splitting pattern of the metal 4f and 5d AOs under D_{3h}^* symmetry. Nevertheless, the band at 17650 cm^{-1} was assigned to the 4f → 5dσ (a_1') transition, which is some 4350 cm^{-1} lower than the lowest previously reported f → d shift in Ce(III) chemistry (Ce^{3+} in $Y_3Al_5O_{12}$ [42]) and is especially remarkable in light of the fact that the lowest excited $4f^05d^1$ state of gaseous Ce(III) lies 49737 cm^{-1} above the ground state [43,44]. It is encouraging that our ($4e_{3/2} + 7e_{1/2} + 8e_{1/2}$) → $12e_{1/2}$ shift should come at 16542 cm^{-1}, only 1100 cm^{-1} away from the value for [Ce(η-$C_5H_3(SiMe_3)_2)_3$].

The experimental transition at 22125 cm^{-1} does not, at first glance, seem to correspond to any of the calculated transition energies. The experimental band was assigned as a 4f → 5dπ (e″) transition. Our calculations suggest an alternative assignment. The addition of two electron-donating $SiMe_3$ functional groups to a Cp ligand is expected to raise the energies of the Cp π orbitals. Thus, the (η-C_5H_5) π_2 → Ce 4f̄ transition, which is calculated at ca. 26500 cm^{-1}, is expected to exhibit a red-shift upon $SiMe_3$ substitution. The experimental band at ca. 22000 cm^{-1} may therefore be due to this type of transition.

The onset of the charge transfer band at ca. 25000 cm^{-1} in the experimental spectrum is matched quite

well by our calculation, although these calculated transitions are expected to be more sensitive to the differences between (η-C_5H_5) and (η-$C_5H_3(SiMe_3)_2$) than are the metal-localised transitions. In particular, the same argument used above would predict that the metal → ligand charge transfer band should exhibit a blue shift upon functionalisation of the rings, and such a change would make the agreement of theory with experiment less impressive. The agreement of our calculated charge transfer onset with the experimental observation may therefore be rather fortuitous.

[Th(η-C_5H_5)$_3$]. The calculated spectrum of [Th(η-C_5H_5)$_3$] is very different from its lanthanide analogue in that the metal-localised transitions all possess 6d/$\bar{\text{d}}$ → predominantly 5$\bar{\text{f}}$ or 5f character, i.e. they are all predicted to have high oscillator strengths. The first two transitions lie at comparatively low energy, with a subsequent gap to a group of three more shifts between ca. 13600 and 15600 cm^{-1}. The $7e_{1/2} \rightarrow 11e_{1/2}$ transition is predicted at 19121 cm^{-1}, with the remaining d → f shift nearly 8000 cm^{-1} higher still in energy. As with [Ce(η-C_5H_5)$_3$], the metal-localised antibonding nature of the $12e_{1/2}$ MO results in a significantly greater transition energy for electron excitation into it. Indeed, the calculation predicts that the $7e_{1/2} \rightarrow 12e_{1/2}$ transition should occur at higher energy than the $7e_{1/2} \rightarrow 6e_{3/2}$ shift, reversing the ground state orbital ordering. The $6e_{3/2}$ MO is a mixture of Th 5f, 6d and (η-C_5H_5) π_3 character, and the $7e_{1/2} \rightarrow 6e_{3/2}$ transition therefore contains aspects of both metal-localised and metal → ligand charge transfer shifts. The ligand → metal $6e_{1/2} \rightarrow 7e_{1/2}$ excitation is calculated to occur within the same energy range as the $7e_{1/2} \rightarrow 6e_{3/2}$ and $7e_{1/2} \rightarrow 12e_{1/2}$ transitions.

The experimental situation for [Th(η-C_5H_5)$_3$] is as for [Ce(η-C_5H_5)$_3$], the spectrum of [Th(η-C_5H_5)$_3$] has not been measured whereas that of [Th(η-$C_5H_3(SiMe_3)_2$)$_3$] does exist [6,45]. It consists of three intense peaks in the 14000–22000 cm^{-1} range, with a fourth peak at 27800 cm^{-1}, which is a shoulder to an extremely intense charge transfer band. No other peaks were recorded as low as 5000 cm^{-1}.

The agreement between the calculated spectrum of [Th(η-C_5H_5)$_3$] and the experimental one of [Th(η-$C_5H_3(SiMe_3)_2$)$_3$] is quantitatively rather poor, in that there are no experimentally found transitions below 14000 cm^{-1}. As both the $7e_{1/2} \rightarrow 4e_{3/2}$ and $7e_{1/2} \rightarrow 8e_{1/2}$ are expected to be intense, it is unlikely that they were simply not observed experimentally. We may, however, attempt a more qualitative comparison with the experimental data. The peaks centred at 15250 and 16950 cm^{-1} are somewhat broader than that at 19800 cm^{-1}, suggesting that more than one transition may be associated with each. Following this reasoning, we may link the $7e_{1/2} \rightarrow 4e_{3/2}$ and $7e_{1/2} \rightarrow 8e_{1/2}$ transitions with the peak at 15250 cm^{-1}. Subsequently we can associate the $7e_{1/2} \rightarrow 9e_{1/2}$, $7e_{1/2} \rightarrow 10e_{1/2}$ and $7e_{1/2} \rightarrow 5e_{3/2}$ shifts with the experimental peak at 16950 cm^{-1}, and the single $7e_{1/2} \rightarrow 11e_{1/2}$ transition with the sharper peak at 19800 cm^{-1}. The quantitative agreement in these latter assignments is superior to that for the first peak.

In making these associations, we are in accord with the experimental assignment, which was to three of the expected four (in D_{3h}^*) 6d → 5f transitions. The experimental assignment of the fourth peak, at 27800 cm^{-1}, however, was less confident, in that associating it with the fourth 6d → 5f transition places the separation of the centres of gravity of the 5f and 5$\bar{\text{f}}$ sets at ca. 9000 cm^{-1}, with a total splitting of the 5f ($j = 7/2$) manifold of more than 12000 cm^{-1}. Both of these values are significantly greater than expected. This line of reasoning, however, is based on the assumption that the transitions are between wholly metal-localised orbitals. Our calculations demonstrate that the splitting of the Th 5f AOs into $j = 5/2$ and $j = 7/2$ manifolds is by no means well defined, and a common theme among all our [M(η-C_5H_5)$_3$] (M = Ln, An) results is the destabilisation of one metal f-based orbital above the rest via interaction with the (η-C_5H_5) π_2 orbitals. We therefore suggest that it is not erroneous to ascribe the peak at 27800 cm^{-1} to a 6d → 5f transition. Whether that transition is to the $7e_{1/2} \rightarrow 12e_{1/2}$ shift at 27053 cm^{-1} or the $7e_{1/2} \rightarrow 6e_{3/2}$ transition at 25461 cm^{-1} is impossible to say; both have significant 6d → 5f character. We feel, however, that it is unnecessary to invoke a possible 6d → 7s shift to explain the peak at 27800 cm^{-1}, as was proposed in the experimental assignment.

The charge transfer band whose onset is at ca. 29000 cm^{-1} was assigned as a metal → ligand transition. It is not possible from our results to confirm or reject this suggestion; we note only that transitions with significant metal → ligand character begin at ca. 25500 cm^{-1} ($7e_{1/2} \rightarrow 6e_{3/2}$) and that the ligand → metal, (η-C_5H_5) $\pi_2 \rightarrow$ Th 6d/$\bar{\text{d}}$, $6e_{1/2} \rightarrow 7e_{1/2}$ shift is calculated to occur at ca. 26500 cm^{-1}. As with the Ce case, it is transitions involving ligand-based orbitals that will vary most between [Th(η-C_5H_5)$_3$] and [Th(η-$C_5H_3(SiMe_3)_2$)$_3$].

3.2. *[Pa(η-C_8H_8)$_2$]*

The electronic structures of the family of [M([8]annulene)$_2$] (M = Th–Pu) molecules have been extensively studied in the 25 years since the initial synthesis of uranocene [46]. These elegant compounds lend themselves to electronic structure determination in that their high symmetry, D_{8h}, separates the contributions of the actinide 6d and 5f AOs to the MOs, facilitating a ready partitioning of their respective involvement in metal–ring bonding. Indeed, the relative contributions of the

metal 6d and 5f AOs to the valence MOs of these compounds has been one of the most widely addressed questions in studies of their electronic structures, with particular emphasis on the extent of metal–ligand covalency.

It is not our intention in this paper to provide another detailed examination of the bonding in actinocenes, as we feel that a consistent picture has emerged in the last few years through a combination of theoretical [16–24] and experimental [25–27] studies. We intend to focus on protactinocene; to calculate its electronic absorption spectrum and to compare it with the experimentally determined spectrum of $[Pa(\eta\text{-}C_8H_4(CH_3)_4)_2]$ [7]. To do so will require some discussion of the MO structure of the molecule, which will also allow comparison of the DV-Xα method with other approaches.

3.2.1. Bonding in $[Pa(\eta\text{-}C_8H_8)_2]$

The results of our non-relativistic and relativistic calculations on $[Pa(\eta\text{-}C_8H_8)_2]$ are presented in Fig. 3. As with $[Ce(\eta\text{-}C_5H_5)_3]$ and $[Th(\eta\text{-}C_5H_5)_3]$, we will initially discuss the non-relativistic calculation, as this

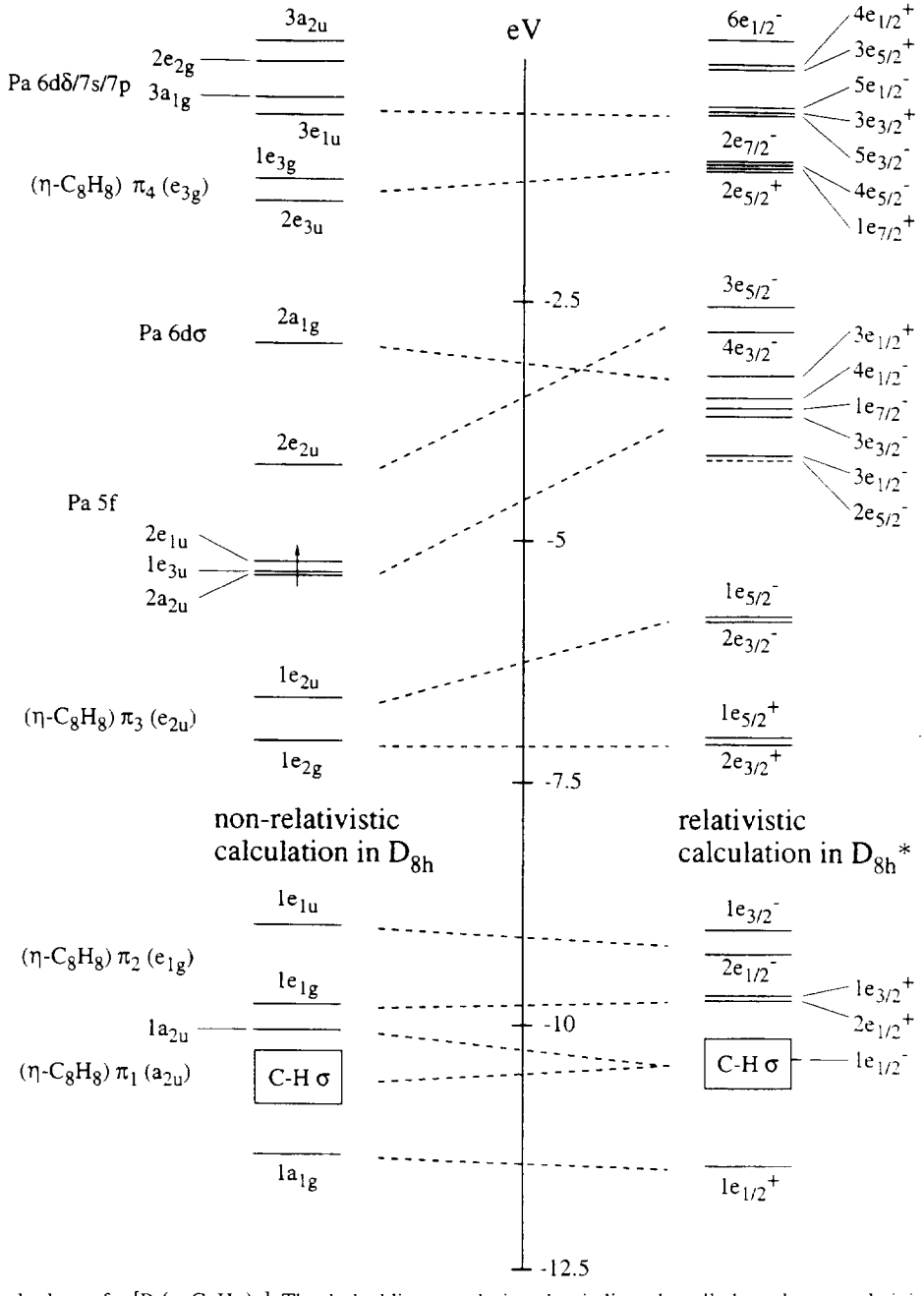

Fig. 3. Molecular orbital scheme for $[Pa(\eta\text{-}C_8H_8)_2]$. The dashed lines are designed to indicate broadly how the non-relativistic MOs relate to their relativistic counterparts.

more clearly illustrates the main features of the metal–ligand bonding. Quantitative considerations, however, are reserved for the relativistic results.

Non-relativistic calculations. The C 2pπ AOs (those oriented parallel to the molecular eight-fold axis) give rise to a_{2u} (π_1), e_{1g} (π_2), e_{2u} (π_3), e_{3g} (π_4) and b_{2u} (π_5) orbitals in D_{8h} symmetry. Completely filling the a_{2u}, e_{1g} and e_{2u} MOs yields $(\eta\text{-}C_8H_8)^{2-}$, which satisfies the Hückel $(4n+2)$ rule for aromaticity [39]. Each ring MO gives rise to two ligand group orbitals, one g and one u, when two $(\eta\text{-}C_8H_8)$ rings interact to generate an $(\eta\text{-}C_8H_8)_2$ D_{8h} ligand field. At most negative eigenvalues on the left-hand side of Fig. 3 come the $1a_{1g}$ and $1a_{2u}$ MOs, which are derived principally from the $(\eta\text{-}C_8H_8)$ π_1 level. These sandwich a block of C–H σ bonding orbitals, in a manner similar to the $(\eta\text{-}C_5H_5)$ π_1-based $1a_1$ and 1e orbitals in $[Ce(\eta\text{-}C_5H_5)_3]$ and $[Th(\eta\text{-}C_5H_5)_3]$. At higher energy are the $1e_{1g}$ and $1e_{1u}$ MOs, which are mainly $(\eta\text{-}C_8H_8)$ π_2 in character, and the filled $1e_{2g}$ and $1e_{2u}$ levels, which are derived from π_3.

In a D_{8h} ligand field, the metal 5f AOs split into a_{2u}, e_{1u}, e_{2u} and e_{3u} sets (fσ, fπ, fδ and fϕ respectively), while the 6d give rise to a_{1g} (dσ), e_{1g} (dπ) and e_{2g} (dδ) levels. Initially it was proposed that a 5fδ/ligand e_{2u} interaction was the primary source of covalent bonding in uranocene [46], but it has subsequently become clear that 6d participation is also important. Conclusive evidence for this interaction came from a variable photon energy photoelectron spectroscopy study on uranocene [27], which unequivocally assigned the $1e_{2g}^{-1}$ band as lying at higher ionisation energy than the $1e_{2u}^{-1}$, indicating a substantial U 6d AO contribution to the $1e_{2g}$ MOs. This result has been confirmed in recent theoretical studies [23,24].

Fig. 3 demonstrates that the metal–ligand interactions in $[Pa(\eta\text{-}C_8H_8)_2]$ are analogous to those in $[U(\eta\text{-}C_8H_8)_2]$. It also indicates that three of the four non-relativistic Pa 5f orbitals lie in a very narrow energy range, and contain the single metal-localised electron. The remaining f-based orbitals, the 5fδ $2e_{2u}$ levels, are significantly destabilised above the other 5f-based MOs, on account of their interaction with the $(\eta\text{-}C_8H_8)_2$ e_{2u} orbitals. The 5f splitting pattern is strong evidence to suggest that this interaction is the only significant source of f-orbital covalency in $[Pa(\eta\text{-}C_8H_8)_2]$.

Above the Pa 5f-based manifold comes the $2a_{1g}$ Pa 6dσ MO. In the $[Ce(\eta\text{-}C_5H_5)_3]$ and $[Th(\eta\text{-}C_5H_5)_3]$ cases, the dσ orbital is found to be the most stable of the metal d manifold, an effect rationalised by its experiencing little interaction with a largely equatorial ligand field. In actinocenes the ligand field is pseudo-axial, and yet the dσ orbital once again has the least involvement with it. Although somewhat counter-intuitive, this result has been obtained in previous actinocene calculations [23], and experimentally in a range of transition metal sandwich molecules containing five-, six- and seven-membered carbocyclic rings [47–51]. In the transition metal complexes, the metal–ring δ interaction is a metal → ligand back-bonding effect, producing a $\delta < \sigma < \pi$ splitting of the metal d-based MOs. The $(\eta\text{-}C_8H_8)_2$ δ (e_{2g}) orbitals are filled, however, producing a destabilisation of the metal 6dδ set and an overall $\sigma < \delta < \pi$ splitting. Nevertheless, in all cases the dσ level is found to be largely metal–ligand non-bonding. This observation has been explained in terms of the metal–ligand overlap [48–51], in that the nodal cone of the d_{z^2} AO intersects the metal-directed lobes of the C 2pπ orbitals close to their region of maximum electron density, giving little net overlap.

Relativistic calculations. As explain in Section 3.1.1, all electronic states in heavy element complexes are properly characterised by non-integral angular momentum values, and must be described via the use of double point groups. The D_{8h}^* double group has eight extra irreducible representations in addition to those of the single group, and all of these have two-fold (Kramers) degeneracy. The most significant effect of spin–orbit coupling in D_{8h} systems, therefore, is a lifting of the degeneracies of the e orbitals. The relationship between the spatial MOs of the D_{8h} point group and the spin-orbitals of the D_{8h}^* double group are given in Table 4.

As observed for $[Ce(\eta\text{-}C_5H_5)_3]$ and $[Th(\eta\text{-}C_5H_5)_3]$, the incorporation of relativity has only minor effects on the largely ligand-based MOs. The $1e_{1/2^+}$ and $1e_{1/2^-}$ orbitals, the relativistic equivalents of the $1a_{1g}$ and $1a_{2u}$, are found to have small metal contributions. It is interesting to note, however, that while the $1a_{2u}$ level has ca. 5% Pa 6p character, the $1e_{1/2^-}$ MO shows mainly 5f and 5f̄ metal content. The Pa 6p AOs are stabilised on the inclusion of relativity, and are therefore expected to mix less with the $(\eta\text{-}C_8H_8)$ valence orbitals. It is likely

Table 4
Relationship between the irreducible representations of the D_{8h} single and D_{8h}^* double point groups

D_{8h}	D_{8h}^*
a_{1g}	$e_{1/2^+}$
a_{2g}	$e_{1/2^+}$
b_{1g}	$e_{7/2^+}$
b_{2g}	$e_{7/2^+}$
e_{1g}	$e_{1/2^+} + e_{3/2^+}$
e_{2g}	$e_{3/2^+} + e_{5/2^+}$
e_{3g}	$e_{5/2^+} + e_{7/2^+}$
a_{1u}	$e_{1/2^-}$
a_{2u}	$e_{1/2^-}$
b_{1u}	$e_{7/2^-}$
b_{2u}	$e_{7/2^-}$
e_{1u}	$e_{1/2^-} + e_{3/2^-}$
e_{2u}	$e_{3/2^-} + e_{5/2^-}$
e_{3u}	$e_{5/2^-} + e_{7/2^-}$

that the removal of the destabilising 6p influence and the inclusion of a small f-orbital contribution are responsible for the slight stabilisation of the $1e_{11/2^-}$ level over the $1a_{2u}$.

The $2e_{1/2^+}$ and $1e_{3/2^+}$ MOs reveal a ca. 10% Pa 6d content, in line with the $1e_{1g}$ level from which they stem. Spin–orbit splitting of the $1e_{1u}$ MO is slightly greater than that of the $1e_{1g}$, and may be traced to the small Pa 7p (and, in the $1e_{3/2^-}$ case, 6p) contributions. Although there is less p character to the $2e_{1/2^-}$ and $1e_{3/2^-}$ MOs than d content in the $2e_{11/2^+}$ and $1e_{3/2^+}$, spin–orbit coupling effects decrease significantly with increasing orbital angular momentum.

This effect is further illustrated by the $2e_{3/2^-}$, $1e_{5/2^-}$ and $2e_{3/2^-}$, $1e_{5/2^-}$ orbital pairs, which show minimal separation in spite of significant 6d and 5f contributions. The $2e_{3/2^-}$ and $1e_{5/2^+}$ orbitals have an almost identical Pa 6d contribution as their $1e_{2g}$ non-relativistic equivalent, at ca. 20%. There is a significant difference, however, between the Pa 5f content of the $2e_{3/2^-}$ and $1e_{5/2^-}$ MOs and the $1e_{2u}$ level. The non-relativistic calculations suggest 31.69% 5f character, while the relativistic orbitals have only 16–18% 5f content. This change is a result of the most significant effect of the inclusion of relativity for the electronic structure of $[Pa(\eta\text{-}C_8H_8)_2]$, namely the destabilisation of the Pa 5f AOs. The destabilisation increases the energetic separation of the 5f AOs from the $(\eta\text{-}C_8H_8)$ π_3 orbitals, with a concomitant reduction in their participation in the metal–ring bonding orbitals. Even this reduced 5f character is sufficient, however, to destabilise the $2e_{3/2^-}$ and $1e_{5/2^-}$ MOs relative to the $1e_{2u}$ level.

It is worth noting at this point that the metal contributions to the $1e_{1/2^+}$–$1e_{5/2^-}$ MOs are extremely similar to the corresponding levels derived from Hartree–Fock–Slater LCAO calculations on $[Pa(\eta\text{-}C_8H_8)_2]$ and the other early actinocenes [23]. Indeed, our calculations agree very closely in nearly all respects with the results of the previous investigation, which suggests that these different density functional methods provide consistent descriptions of the electronic structures of actinide-containing molecules.

There are some similarities between the metal-localised MOs of $[Pa(\eta\text{-}C_8H_8)_2]$ and those of $[Th(\eta\text{-}C_5H_5)_3]$. As with the tris $(\eta\text{-}C_5H_5)$ compound, there is no clear three-below-four splitting pattern of the $2e_{5/2^-}$–$3e_{5/2^-}$ Pa 5f-based MOs, although 5f character is predominant in the $2e_{5/2^-}$, $3e_{1/2^-}$ and $3e_{3/2^-}$ levels. The relativistic equivalents of the $2e_{2u}$ MO, the $4e_{3/2^-}$ and $3e_{5/2^-}$ orbitals, are destabilised above the other f-based levels on account of their metal–ligand antibonding nature.

As with $[Th(\eta\text{-}C_5H_5)_3]$, the incorporation of relativity slightly stabilises the Pa $6d_{z^2}$-based $2a_{1g}$ orbital by increasing the percentage of Pa 7s character. This effect combines with the destabilisation of the 5f manifold to bring the f-based MOs and $6d\sigma$ level closer in energy. In $[Th(\eta\text{-}C_5H_5)_3]$ this effect is sufficient to cause the formal ground state of the molecule to be $6d^1$. There is a bigger initial gap between the 6d and 5f AOs in Pa, however, as the 5f orbitals are progressively stabilised with increasing atomic number [52,53], and the inclusion of relativity in $[Pa(\eta\text{-}C_8H_8)_2]$ does not alter the ground electronic configuration, i.e. both non-relativistic and relativistic calculations predict a formal $5f^1$ system. Instead the $6d\sigma$-based orbital, the $3e_{1/2^+}$, is now right in the heart of the 5f manifold, suggesting that there should be a low-energy f → d transition in $[Pa(\eta\text{-}C_8H_8)_2]$. It is to this, and the rest of the predicted electronic absorption spectrum, that we now turn.

3.2.2. Electronic excitation energies in $[Pa(\eta\text{-}C_8H_8)_2]$

The $2e_{5/2^-}$ and $3e_{1/2^-}$ MOs of $[Pa(\eta\text{-}C_8H_8)_2]$ are almost degenerate, with only 0.001 eV separating them.

Table 5
Calculated relativistic electronic transition energies in $[Pa(\eta\text{-}C_8H_8)_2]$; experimental values for $[Pa(\eta\text{-}C_8H_4(CH_3)_4)_2]$ from Ref. [7]

Transition	Transition type [a]	Energy
(i) $[Pa(\eta\text{-}C_8H_8)_2]$, calculated		
$(2e_{5/2^-} + 3e_{1/2^-}) \rightarrow 3e_{3/2^-}$	Pa $5\bar{f} \rightarrow$ Pa $5\bar{f}/5f$	4002 cm^{-1} (0.496 eV)
$(2e_{5/2^-} + 3e_{1/2^-}) \rightarrow 1e_{7/2^-}$	Pa $5\bar{f} \rightarrow$ Pa 5f	4247 cm^{-1} (0.523 eV)
$(2e_{5/2^-} + 3e_{1/2^-}) \rightarrow 4e_{1/2^-}$	Pa $5\bar{f} \rightarrow$ Pa 5f	5375 cm^{-1} (0.666 eV)
$(2e_{5/2^-} + 3e_{1/2^-}) \rightarrow 3e_{1/2^-}$	Pa $5\bar{f} \rightarrow$ Pa $6d/6\bar{d}$	10973 cm^{-1} (1.360 eV)
$(2e_{5/2^-} + 3e_{1/2^-}) \rightarrow 4e_{3/2^-}$	Pa $5\bar{f} \rightarrow$ Pa $5f/5\bar{f}$	11293 cm^{-1} (1.400 eV)
$(2e_{5/2^-} + 3e_{1/2^-}) \rightarrow 3e_{5/2^-}$	Pa $5\bar{f} \rightarrow$ Pa 5f	13589 cm^{-1} (1.685 eV)
$1e_{5/2^-} \rightarrow (2e_{5/2^-} + 3e_{1/2^-})$	$(\eta\text{-}C_8H_8)\pi_3 \rightarrow$ Pa $5\bar{f}$	21398 cm^{-1} (2.653 eV)
$1e_{5/2^-} \rightarrow (2e_{5/2^-} + 3e_{1/2^-})$	$(\eta\text{-}C_8H_8)\pi_3 \rightarrow$ Pa $5\bar{f}$	27749 cm^{-1} (3.440 eV)
$(2e_{5/2^-} + 3e_{1/2^-}) \rightarrow 4e_{5/2^-}$	Pa $5\bar{f} \rightarrow (\eta\text{-}C_8H_8)\pi_4$	28508 cm^{-1} (3.535 eV)
$(2e_{5/2^-} + 3e_{1/2^-}) \rightarrow 2e_{5/2^-}$	Pa $5\bar{f} \rightarrow (\eta\text{-}C_8H_8)\pi_4$	29750 cm^{-1} (3.689 eV)
(ii) $[Pa(\eta\text{-}C_8H_4(CH_3)_4)_2]$, experimental		
	charge transfer	20400 cm^{-1}
	charge transfer	26300 cm^{-1}

[a] Unbarred labels refer to the higher angular momentum j-based atomic orbital, barred to the lower.

As with $[Ce(\eta\text{-}C_5H_5)_3]$ it was therefore necessary to employ a thermal spreading factor to converge the $[Pa(\eta\text{-}C_8H_8)_2]$ calculations, partitioning the single f-based electron between the $2e_{5/2^-}$ and $3e_{1/2^-}$ orbitals. Transition energies were calculated in the same way as for $[Ce(\eta\text{-}C_5H_5)_3]$, described in Section 3.1.2.

The calculated spectrum is presented in Table 5. It shows three low-energy primarily $\bar{f} \rightarrow f$ transitions, at 4002, 4237 and 5375 cm^{-1}. Subsequently there is a gap to the excitation at 10973 cm^{-1}, the $5\bar{f} \rightarrow 6d/6\bar{d}$ transition discussed in Section 3.2.1. This $f \rightarrow d$ shift is at even lower energy than the equivalent in $[Ce(\eta\text{-}C_5H_5)_3]$, and is an example of how potentially fascinating the absorption spectroscopy of Pa^{4+} compounds should be, given the energetic proximity of the metal valence AOs. As noted previously [1,6], the scarcity and radioactivity of Pa severely hampers its study.

Almost isoenergetic with the $f \rightarrow d$ transition is the first of the two excitations to the metal–ring antibonding $4e_{3/2^-}$ and $3e_{5/2^-}$ MOs. These are separated by ca. 2300 cm^{-1}, at 11293 and 13589 cm^{-1} respectively. As noted for $[Ce(\eta\text{-}C_5H_5)_3]$, it is the energy of the $f \rightarrow d$ transition that differs most between ground and transition state calculations. The gap between the $2e_{5/2^-}$ and $3e_{1/2^+}$ MOs is 6952 cm^{-1} in the ground state calculation, significantly less than the predicted $f \rightarrow d$ transition. The essentially $f \rightarrow f$ transition MO energy differences, however, are more closely matched in the two calculation types.

The first transition with significant charge transfer character is predicted to lie well removed from the metal-localised transitions, the mainly $(\eta\text{-}C_8H_8)\pi_3 \rightarrow$ Pa $5\bar{f}$, $1e_{5/2^-} \rightarrow (2e_{5/2^-} + 3e_{1/2^-})$ shift being calculated at 21398 cm^{-1}. Hence the spectrum of $[Pa(\eta\text{-}C_8H_8)_2]$ is predicted to be free of charge transfer transitions until well after the metal-based transitions have occurred.

In D_{8h}^*, none of the $f \rightarrow f$ transitions is symmetry-allowed, and consequently they are expected to be very weak. The $2e_{5/2^-} \rightarrow 3e_{1/2^+}$ is also symmetry-forbidden, but the $3e_{1/2^-} \rightarrow 3e_{1/2^-}$ is allowed (the direct product of the $e_{1/2^-}$ and $e_{1/2^+}$ irreducible representations spans both components of the dipole moment operator). Hence the $f \rightarrow d$ transition is fully allowed, and is expected to be intense. This $f \rightarrow d$ transition may well mask the energetically similar $(2e_{5/2^-} + 3e_{1/2^-}) \rightarrow 4e_{3/2^-}$ and $(2e_{5/2^-} + 3e_{1/2^-}) \rightarrow 3e_{5/2^-}$ transitions, thus making them impossible to detect.

The optical spectrum of $[Pa(\eta\text{-}C_8H_4(CH_3)_4)_2]$ [7] shows a single band at 380 nm (26300 cm^{-1}) with a shoulder at 490 nm (20400 cm^{-1}) (Table 5). It was noted that the spectrum resembled that of thorocene. Thorocene possesses no metal-based electrons and consequently its optical spectrum must consist of ligand → metal charge transfer transitions. The results of our calculations and the experimental similarity of the spectra of thorocene and $[Pa(\eta\text{-}C_8H_4(CH_3)_4)_2]$ suggest that the latter's spectrum be interpreted in terms of charge transfer transitions. Indeed, our calculation of ligand → metal charge transfer transitions at 21398 and 27749 cm^{-1} and metal → ligand transitions beginning at 28500 cm^{-1} is in close agreement with the experimental values for $[Pa(\eta\text{-}C_8H_4(CH_3)_4)_2]$.

It is extremely unlikely that the experimental spectrum involves the $f \rightarrow d$ transition, for our calculation would then be some 15000 cm^{-1} in error. Support for this assertion comes from the experimental spectrum of uranocene, in which the $5f^2 \rightarrow 5f^16d^1$ transitions span the energy range 15170–16270 cm^{-1} [26]. That the lowest energy $5f^2 \rightarrow 5f^16d^1$ transition in free U^{4+} [54] is some 10000 cm^{-1} greater than the $5f^1 \rightarrow 6d^1$ shift in Pa^{4+} [55] is entirely consistent with our prediction of the equivalent transition in protactinocene lying at lower energy than in uranocene. We feel confident, therefore, in suggesting that the $f \rightarrow d\sigma$ transition in a protactinocene has yet to be experimentally observed, and should lie in the near infrared at ca. 11000 cm^{-1}.

4. Summary and conclusions

The factors that cause the differences between the ground state electronic structures of $[Ce(\eta\text{-}C_5H_5)_3]$ and $[Th(\eta\text{-}C_5H_5)_3]$ have important consequences for their electronic absorption spectra. The non-relativistic calculations indicate formal configurations of $4f^1$ and $5f^1$ for $[Ce(\eta\text{-}C_5H_5)_3]$ and $[Th(\eta\text{-}C_5H_5)_3]$ respectively. Inclusion of relativity destabilises the nf orbitals and slightly stabilises the $(n+1)d\sigma$, with the result that the ground configuration of $[Th(\eta\text{-}C_5H_5)_3]$ is formally $6d^1$. The energetic proximity of the nf and $(n+1)d\sigma$ orbitals, generated by a combination of relativistic effects and a site symmetry with no axial ligands, results in a very low $f \rightarrow d$ transition energy in $[Ce(\eta\text{-}C_5H_5)_3]$, while for $[Th(\eta\text{-}C_5H_5)_3]$ the predicted spectrum involves a host of $d \rightarrow f$ transitions. In $[Ce(\eta\text{-}C_5H_5)_3]$ the 4f AOs are little perturbed from those of free Ce(III), with the prediction of four essentially $\bar{f} \rightarrow f$ transitions (promotion of the $j = 5/2$ electron to the $j = 7/2$ manifold) prior to the $\bar{f} \rightarrow d\sigma$ shift. In $[Th(\eta\text{-}C_5H_5)_3]$ the greater radial extension of the 5f orbitals and their energetic proximity to the $(\eta\text{-}C_5H_5)\pi_3$ and remaining metal valence orbitals results in a less atom-like distribution of levels to which promotion of the $6d^1$ electron occurs.

In agreement with previous studies, a substantial degree of metal–ligand covalency has been found to the bonding in $[Pa(\eta\text{-}C_8H_8)_2]$, involving both the Pa 6d ($1e_{1g}$ and $1e_{2g}$) and 5f ($1e_{2u}$) orbitals. As with $[Th(\eta\text{-}C_5H_5)_3]$, the three-below-four spin–orbit coupling pattern of the 5f manifold, expected of free Pa(IV), is not well defined in $[Pa(\eta\text{-}C_8H_8)_2]$ on account of appreciable metal–ligand mixing. The vacant $6d\sigma$-based MO of $[Pa(\eta\text{-}C_8H_8)_2]$ lies very close in energy to the 5f-based

levels, and the predicted electronic absorption spectrum consists not only of a series of f → f transitions, but also a very low-energy f → d shift. An interpretation of the experimental spectrum of $[Pa(\eta\text{-}C_8H_4(CH_3)_4)_2]$ in terms of both ligand → metal and metal → ligand charge transfer transitions has been presented.

This contribution, in conjunction with our earlier one [1], demonstrates the utility of relativistic density functional theory with respect to the calculation of optical transition energies in f^1 complexes. We are hopeful that these methods can also be applied to f^n $(n > 1)$ complexes, such as those of U(III) and U(IV) and the trivalent later actinides. Such investigations will add the complication of interactions between the metal-localised electrons to the already complex situation discussed here.

Acknowledgements

This work was carried out while NK was a University Postdoctoral Fellow at the Ohio State University. The authors therefore wish to thank the Graduate School of The Ohio State University for a Postdoctoral Fellowship to NK. This work was supported by grants from the Division of Chemical Sciences, Office of Basic Energy Sciences, US Department of Energy (Grant DE-FG02-86ER13529), and from the Ohio Supercomputing Centre.

References and notes

[1] N. Kaltsoyannis and B.E. Bursten, *Inorg. Chem.*, *34* (1995) 2735.
[2] D.E. Ellis, *J. Phys. B: Atom. Molec. Phys.*, *10* (1977) 1.
[3] W.F. Schneider, *Ph.D. Dissertation*, The Ohio State University, 1991.
[4] W.F. Schneider, R.J. Strittmatter, B.E. Bursten and D.E. Ellis, *Density Functional Methods in Chemistry* Springer-Verlag, New York, 1991, Chap. 16.
[5] W.K. Kot, G.V. Shalimoff, N.M. Edelstein, M.A. Edelman and M.F. Lappert, *J. Am. Chem. Soc.*, *110* (1988) 986.
[6] W.K. Kot, *Electronic structure in the actinides – three case studies*, Lawrence Berkeley Laboratory, University of California, 1991.
[7] J.P. Solar, H.P.G. Burghard, R.H. Banks, A. Streitwieser and D. Brown, *Inorg. Chem.*, *19* (1980) 2186.
[8] B.E. Bursten, L.F. Rhodes and R.J. Strittmatter, *J. Am. Chem. Soc.*, *111* (1989) 2756.
[9] B.E. Bursten, L.F. Rhodes and R.J. Strittmatter, *J. Am. Chem. Soc.*, *111* (1989) 2758.
[10] B.E. Bursten, L.F. Rhodes and R.J. Strittmatter, *J. Less-Common Met.*, *149* (1989) 207.
[11] R.J. Strittmatter and B.E. Bursten, *J. Am. Chem. Soc.*, *113* (1991) 552.
[12] P.N. Hazin, J.W. Bruno and H.G. Brittain, *Organometallics*, *6* (1987) 913.
[13] J.V. Ortiz and R. Hoffmann, *Inorg. Chem.*, *24* (1985) 2095.
[14] H. Rabaa, J. Saillard and R. Hoffmann, *J. Am. Chem. Soc.*, *108* (1986) 4327.
[15] L.J. Nugent, P.G. Laubereau, G.K. Werner and K.L. van der Sluis, *J. Organomet. Chem.*, *27* (1971) 365.
[16] H. Amberger, R.D. Fischer and B. Kanellakopoulos, *Theoret. Chim. Acta (Berlin)*, *37* (1975) 105.
[17] R.G. Hayes and N.M. Edelstein, *J. Am. Chem. Soc.*, *94* (1972) 8688.
[18] P. Pyykkö and L.L. Lohr, *Inorg. Chem.*, *20* (1981) 1950.
[19] N. Rösch and A. Streitwieser, *J. Organomet. Chem.*, *145* (1978) 195.
[20] N. Rösch and A. Streitwieser, *J. Am. Chem. Soc.*, *105* (1983) 7237.
[21] N. Rösch, *Inorg. Chim. Acta*, *94* (1984) 297.
[22] P.M. Boerrigter, *Ph.D. Thesis*, Vrije Universiteit, Amsterdam, 1987.
[23] P.M. Boerrigter, E.J. Baerends and J.G. Snijders, *Chem. Phys.*, *122* (1988) 357.
[24] A.H.H. Chang and R.M. Pitzer, *J. Am. Chem. Soc.*, *111* (1989) 2500.
[25] A. Streitwieser, U. Müller-Westerhoff, U.G. Sonnischen, D.G. Mares, K.O. Hodgson and C.A. Harmon, *J. Am. Chem. Soc.*, *95* (1973) 8644.
[26] R.F. Dallinger, P. Stein and T.G. Spiro, *J. Am. Chem. Soc.*, *100* (1978) 7865.
[27] J.B. Brennan, J.C. Green and C.M. Redfern, *J. Am. Chem. Soc.*, *111* (1989) 2373.
[28] A. Avdeef, K.N. Raymond, K.O. Hodgson and A. Zalkin, *Inorg. Chem.*, *11* (1972) 1083.
[29] S.D. Stults, R.A. Andersen and A. Zalkin, *Organometallics*, *9* (1990) 115.
[30] P.C. Blake, M.F. Lappert, J.L. Atwood and J. Zhang, *J. Chem. Soc., Chem. Commun.*, (1986) 1148.
[31] J.W. Lauher and R. Hoffmann, *J. Am. Chem. Soc.*, *98* (1976) 1729.
[32] Unless otherwise stated, the orbital labels under D_{3h} symmetry are given in parentheses.
[33] K.S. Pitzer, *Acc. Chem. Res.*, *8* (1979) 271.
[34] P. Pyykkö, *Acc. Chem. Res.*, *8* (1979) 276.
[35] P. Pyykkö, *Chem. Rev.*, *88* (1988) 563.
[36] In our earlier scattered wave $X\alpha$ calculations [11], the energies of the 4f-based MOs of $[Ce(\eta\text{-}C_5H_5)_3]$ were found to be similar to the equivalent orbitals of $[Np(\eta\text{-}C_5H_5)_3]$, while those of the 5d-based levels matched the 6d-based MOs of $[Pu(\eta\text{-}C_5H_5)_3]$, i.e. the energies of the metal-based valence levels of $[M(\eta\text{-}C_5H_5)_3]$ complexes for the early lanthanides are more akin to the mid actinides than the first 5f elements.
[37] J.A. Salthouse and M.J. Ware, *Point group character tables and related data*, Cambridge University Press, London, 1972.
[38] The HOMOs of the non-relativistic calculations are indicated by a vertical arrow representing the single unpaired electron. The arrow notation implies a direction of electron spin, arrows pointing up are usually taken to represent α spin electrons and those pointing down β spin electrons. Such a representation is conceptually incorrect for the HOMOs of the relativistic calculations as electron spin is incorporated in the symmetry labels of the orbitals. The relativistic HOMOs are therefore represented by a dashed horizontal line.
[39] F.A. Cotton, *Chemical Applications of Group Theory*, Wiley-Interscience, New York, 1991.
[40] From now on, unless otherwise stated, f is taken to mean the total f orbital (i.e. $f+\bar{f}$) to a given MO (and similarly for the other AOs).
[41] J.C. Slater, *The Calculation of Molecular Orbitals*, Wiley, New York, 1979.
[42] W.J. Miniscales, J.M. Pellegrino and W.M. Yen, *J. Appl. Phys.*, *49* (1978) 6109.
[43] R.J. Lang, *Can. J. Res.*, *14A* (1936) 127.
[44] L. Brewer, *J. Opt. Soc. Am.*, *61* (1971) 1666.

[45] [Th(η-C_5H_5)$_3$] has not been synthesised. It is likely that [Th(η-$C_5H_3(SiMe_3)_2$)$_3$] is stable only by virtue of the steric bulk of the (η-$C_5H_3(SiMe_3)_2$) ligands.
[46] A. Streitwieser and U. Müller-Westerhof, *J. Am. Chem. Soc.*, *90* (1968) 7364.
[47] F.G.N. Cloke, A.N. Dix, J.C. Green, R.N. Perutz and E.A. Seddon, *Organometallics*, *2* (1983) 1150.
[48] C.E. Davies, I.M. Gardiner, P.D. Grebenik, J.C. Green, M.L.H. Green, N.J. Hazel, V.S. Mtetwa and K. Prout, *J. Chem. Soc., Dalton Trans.*, (1985) 669.
[49] J.G. Brennan, G. Cooper, J.C. Green, N. Kaltsoyannis, M.A. MacDonald, M.P. Payne, C.M. Redfern and K.H. Sze, *Chem. Phys.*, *164* (1992) 271.
[50] J.C. Green, M.L.H. Green, N. Kaltsoyannis, P. Mountford, P. Scott and S.J. Simpson, *Organometallics*, *11* (1992) 3353.
[51] J.C. Green, N. Kaltsoyannis, M.A. MacDonald and K.H. Sze, *J. Am. Chem. Soc.*, *116* (1994) 1994.
[52] J.-P. Desclaux, *At. Data Nucl. Data Tables*, *12* (1973) 311.
[53] P. Pyykkö and L. Laaksonen, *J. Phys. Chem.*, *88* (1984) 4892.
[54] M.S. Fred and J. Blaise, *The chemistry of the actinide elements*, Vol. 2, Chapman and Hall, New York, 1986, Chap. 15.
[55] N.M. Edelstein, *Eur. J. Solid State Inorg. Chem.*, *28* (1991) 47.